The sensitivity to polarization in stratospheric aerosol retrievals from limb scattered sunlight measurements

B. J. Elash, A. E. Bourassa, L. A. Rieger, S. R. Dueck, D. J. Zawada, and D. A. Degenstein

Contact Author: B. J. Elash, brenden.elash@usask.ca

Institute of Space and Atmospheric Science, 116 Science Place, Saskatoon SK, Canada, S7N 5E2

Keywords: stratosphere, aerosol, limb scattering, retrieval, polarization

Abstract: Satellite measurements of limb scattered sunlight at visible and near infrared wavelengths have been used successfully for several years to retrieve the vertical profile of stratospheric aerosol extinction coefficient. The existing satellite measurements are of the total radiance, with very little knowledge or impact of the polarization state of the limb radiance. Recently proposed instrument concepts for stratospheric aerosol profiling have been designed to measure the linearly polarized radiance. Yet, to date, the impact of the polarized measurement on the retrievals has not been systematically studied. Here we use a fully spherical, multiple scattering radiative transfer model to perform a sensitivity study on the effects of the polarized measurement on stratospheric aerosol extinction retrievals through specific investigations of the aerosol signal fraction in polarized measurements, potential retrieval bias, and achievable precision. In this study, we simulate both total and linearly polarized measurements, for a wide range of limb viewing geometries that are encountered in typical low earth orbits and for various aerosol loading scenarios. The orientation of the linear polarization with respect to the horizon is also studied. Taking into account instrument signal to noise levels it is found that in general, the linear polarization can be used as effectively as the total radiance measurement, with consideration of instrument signal to noise capabilities; however the horizontal polarization is more promising in terms of signal magnitude.

1 Introduction

Stratospheric aerosols, which are submicron-sized spherical liquid droplets of sulfuric acid, cause a cooling effect by scattering the incoming solar irradiance and therefore have an important radiative effect on climate. This effect depends strongly on the aerosol concentration, composition, and particle size distribution (Kiehl and Briegleb, 1993; Stocker et al., 2013) [1, 2]. Recent studies have proposed a link between the so-called global warming hiatus and an increase in the stratospheric sulfate aerosol layer. (Solomon et al., 2011; Haywood et al., 2014; Fyfe et al., 2013) [3, 4, 5]. The increase in stratospheric aerosol over the last decade was primarily caused by a series of minor, mostly tropical volcanic eruptions (Vernier et al., 2011) [6] although the impact of anthropogenic pollution sources continues to be studied (Neely et al, 2014) [7]. As noted in the recent review paper by Kremser et al., 2015, [8] there is a distinct

need for continued monitoring with global coverage of aerosol, particularly extending down to tropopause altitudes.

Stratospheric aerosol distributions have been monitored on a global scale since the 1970s with satellite instruments using a variety of remote sensing techniques. The first satellite aerosol extinction profile retrievals were from limb sounding solar occultation measurements, most notably from the NASA SAGE missions (Russell and McCormick, 1989; Thomason and Taha, 2003) [9, 10]. The solar occultation technique has provided a robust and reliable method to retrieve aerosol extinction by directly measuring the atmospheric transmittance. However, the measuring frequency of occultation measurements is limited due the necessity of a sunrise or sunset and typically requires months to cover a large range of latitudes. Limb scatter measurements, such as from OSIRIS (Llewellyn et al., 2004) [11], SCIAMACHY (Bovensmann et al., 1999) [12], and most recently from OMPS (Rault and Loughman, 2013) [13], have better coverage by only requiring the sunlit conditions at the tangent point, but the retrieval of aerosol is more complex requiring computationally heavy forward modelling and inversion compared to occultation (Bourassa et al., 2007, Bourassa et al., 2012b, Rieger et al., 2014) [14, 15, 16]. It is worthwhile to note the success of limb scatter aerosol measurements: The combination of the SAGE II and OSIRIS datasets have recently been used to successfully create a single long term merged time series depicting the evolution of the stratospheric aerosol layer (Rieger et al., 2015) [17], and OSIRIS measurements have been used as one of primary extensions of the stratospheric aerosol record for the CMIP6 study (Thomason et al., in preparation) [18].

OSIRIS, SCIAMACHY, and OMPS-LP measure the spectral radiance of the scattered sunlight from the limb and use non-linear inversion techniques to retrieve aerosol extinction profiles (Bourassa et al., 2012b; Ernst et al., 2012, Rault and Loughman, 2013) [15, 19, 13]. For these retrievals, some assumptions regarding particle size distributions and/or composition are always required in the forward model. Most importantly for this study, currently none of these retrievals account for any polarization sensitivity in their respective measurements. However, these instruments have been specifically designed to measure the total radiance by minimizing the instrument sensitivity to polarization. Recently proposed instruments with the capability to measure aerosol using limb scattering include the Belgian instrument Atmospheric Limb Tracker for the Investigation of the Upcoming Stratosphere (ALTIUS) (Dekemper et al., 2012; Fussen et al., 2016) [20, 21] and the Aerosol Limb Imager (ALI), a Canadian endeavour (Elash et al., 2016) [22]. Both instruments image the limb and use acousto-optic tunable filters to select the measured wavelength. The use of the acousto-optic filter inherently means that the measured image is of the linearly polarized radiance due to the phonon-phonon interaction that selects the filtered wavelength. Although it has been previously shown that the retrieval of stratospheric aerosol extinction profiles from polarized scattered sunlight measurements are possible (Elash et al., 2016; McLinden et al., 1999) [22, 23], the full impact of the polarized measurement has not been systematically studied. In this work we perform an analysis with simulated polarized measurements to determine first if there are any clear advantages or disadvantages to making the linearly polarized measurement. Further, we investigate which linear polarization and viewing geometries have the largest sensitivities to aerosol, and how the polarized measurements affect the accuracy and precision of the retrieved aerosol product.

2 Background and Forward Model

In order to investigate the effect of polarization on the sensitivity to aerosol, an accurate model of the polarized limb radiance must be employed. Additionally, a large number of scenarios, including various atmospheric states and viewing geometries, are required to fully probe the solution space. In this section, the basic background describing the polarization state of the limb signal is developed, and the SASKTRAN High Resolution (SASKTRAN-HR) model and the various model scenarios used for the analysis are described. Based on the useful spectral range for limb scatter observations of stratospheric aerosol, we have limited our discussion to wavelengths from 500-1500 nm.

2.1 Polarized Scattered Sunlight and Stratospheric Aerosols

The time-averaged polarization state of partially polarized, incoherent light can be fully characterized by a Stokes vector,

$$\boldsymbol{I} = \begin{bmatrix} I \\ Q \\ U \\ V \end{bmatrix} \quad (1)$$

where the coefficients of the Stokes vector, defined in a reference frame, are measures of the total radiance, I, the difference between horizontal polarization to vertical polarization, Q, the difference between +45° diagonal polarization to -45° polarization, U, and the difference between the counter clockwise circular polarization to clockwise polarization, V. Scattering events modify the polarization state of scattered light. This modification is described by a scattering matrix, which is valid for Stokes vectors defined in a scattering frame. Using a reference frame where the x-axis is defined to be the horizontal polarization and where x and y axes are orthogonal leads to the following definition for the Stokes parameters

$$\begin{aligned} I &= <E_x>^2 + <E_y>^2 \\ Q &= <E_x>^2 - <E_y>^2 \\ U &= 2\mathrm{Re}\left(<E_x><E_y^*>\right) \\ V &= -2\mathrm{Im}\left(<E_x><E_y^*>\right). \end{aligned} \quad (2)$$

The polarization state of light propagating along a ray is stored as a Stokes vector defined in some reference frame. When a scattering event is modelled the Stokes vector is rotated into the scattering frame, multiplied by the scattering matrix, and then rotated into a reference frame in which the scattered Stokes vector is stored and is represented by the following operation,

$$\boldsymbol{I}^{sca} = \boldsymbol{L}(\theta_2)\boldsymbol{P}(\Theta)\boldsymbol{L}(\theta_1)\boldsymbol{I}^{inc}. \quad (3)$$

The outgoing, or scattered, and incoming radiances are represented 4 by 1 matrices, i.e. Stokes column vectors, given by $\boldsymbol{I}^{sca}$ and $\boldsymbol{I}^{inc}$, the rotation matrices are denoted $\boldsymbol{L}$ and rotate the incoming ray and scattered ray by rotation angles θ_1 and θ_2. The 4 by 4 scattering matrix is represented by $\boldsymbol{P}(\Theta)$ and is related to the probability that an incoming ray will be scattered at a scattering angle, Θ. It also describes the change in polarization state through the elements of the matrix. The product $\boldsymbol{L}(\theta_2)\boldsymbol{P}(\Theta)\boldsymbol{L}(\theta_1)$ is sometimes referred to as the phase matrix.

For this work, two primary scattering interactions induce and/or modify the polarization state of the light propagating in the atmosphere. These are scattering by the molecular air density and by stratospheric sulfate aerosols. The molecular atmosphere interaction is referred to as Rayleigh scattering, and has a scattering matrix that is determined from the Rayleigh-Gans approximation (Mishchenko et al., 2002) [24] given by

$$\boldsymbol{P}(\boldsymbol{\Theta})_{\boldsymbol{ray}} = \frac{3}{4}\begin{bmatrix} 1+\cos^2\Theta & -\sin^2\Theta & 0 & 0 \\ -\sin^2\Theta & 1+\cos^2\Theta & 0 & 0 \\ 0 & 0 & 2\cos\Theta & 0 \\ 0 & 0 & 0 & 2\cos\Theta \end{bmatrix} \quad (4)$$

where Θ is the scattering angle.

For randomly orientated or spherical particles, such as stratospheric aerosol, only six elements of the scattering matrix are required (van de Hulst, 1957) [25] which are the following

$$\boldsymbol{P}(\boldsymbol{\Theta}) = \begin{bmatrix} P_{11}(\Theta) & P_{12}(\Theta) & 0 & 0 \\ P_{12}(\Theta) & P_{22}(\Theta) & 0 & 0 \\ 0 & 0 & P_{33}(\Theta) & P_{34}(\Theta) \\ 0 & 0 & -P_{34}(\Theta) & \mathrm{P}_{44}(\Theta) \end{bmatrix} \quad (5)$$

Additionally, for spherical particles like stratospheric aerosol only four unique terms are required since $P_{11} = P_{22}$ and $P_{33} = P_{44}$. Spherical aerosol scattering at visible and near-infrared wavelengths is fully described by Mie theory (Mie, 1908) [26], for which several standard codes have been developed to calculate scattering cross sections and scattering matrices based on the particle size distribution and index of refraction (e.g. Wiscombe, 1980) [27]. A full derivation can be found in van de Hulst (1957) [25].

The basic polarization state of the scattered light in the Earth's atmosphere can be understood by first considering a single scattering event of the unpolarized incoming sunlight in a molecular atmosphere. For reference, the Solar Scattering Angle (SSA) is defined to be the angle between the direction to the sun and the line of sight. It can be easily seen from the form of the Rayleigh scattering matrix (Equation 4) that a single scattering event causes the sky to develop a distinct polarization at a SSA of 90 degrees from the incoming solar beam. Note that the horizontal and vertical polarizations are given by $0.5(I+Q)$ and $0.5(I+Q)$ respectively. The scattered sunlight is linearly polarized in the horizontal orientation, which is parallel to the horizon. The degree of polarization gradually decreases at scattering angles greater than or less than 90 degrees (broadly referred to as back-scatter and forward-scatter geometries, respectively). In this single scattering scenario, the radiance is completely unpolarized at SSAs of 0 and 180 degrees. If multiple scattering events are taken into account, the degree of polarization is decreased at 90 degrees SSA, and conversely does not become completely unpolarized at SSAs of 0 and 180 degrees. Simulations with the SASKTRAN-HR radiative transfer model, which is described below, using an atmosphere of molecular air density show that at 90 degrees SSA, the degree of linear polarization of the limb radiance is approximately 95% for a wavelength of 750 nm. This linear polarization effect is strongest at longer wavelengths (i.e. approaching 1500 nm) and decreases, on average by 10%, as the wavelength become shorter (i.e. down to 500 nm). This is directly related to the greater contribution from multiple scattering at shorter wavelengths. As the SSA increases from 90 degrees, the degree of linear polarization decreases. It is approximately 20% for a back scatter geometry of 180 degrees, and 30% for a scattering angle of 45 degrees. The ratio of the horizontal polarization over the total radiance and the vertical polarization over

the total radiance is shown in the top of Figure 1. The strong polarized nature can be noticed around the SSA of 90 degrees where the radiance is almost completely horizontally polarized.

For an atmosphere that contains both the molecular air density as well as a typical background state of stratospheric sulfate aerosol, both Rayleigh and Mie scattering occur in a weighted fraction determined by the optical depth of air and aerosol. Compared to the pure Rayleigh scattering case, the addition of aerosol causes a decrease in the degree of linear horizontal polarization for wavelengths shorter than approximately 750 nm. The bottom two panels of Figure 1 show the difference in the ratio of the polarized over the total radiance for the atmosphere with aerosol and the one without, demonstrating that this effect has a weak dependence on SSA, with the most depolarization occurring in forward scatter geometries for short wavelengths. Interestingly, for longer wavelengths in back-scatter geometries, the opposite occurs. This is due to the changing fraction of scattering from the molecular air density and aerosol because the Rayleigh scattering cross section falls off much more quickly with wavelength than the aerosol cross section. The magnitude of the observed change in linear polarization from a pure Rayleigh atmosphere to that with typical background aerosol is approximately 5-10%, but it obviously varies depending on the aerosol loading and the microphysical parameters of the aerosol.

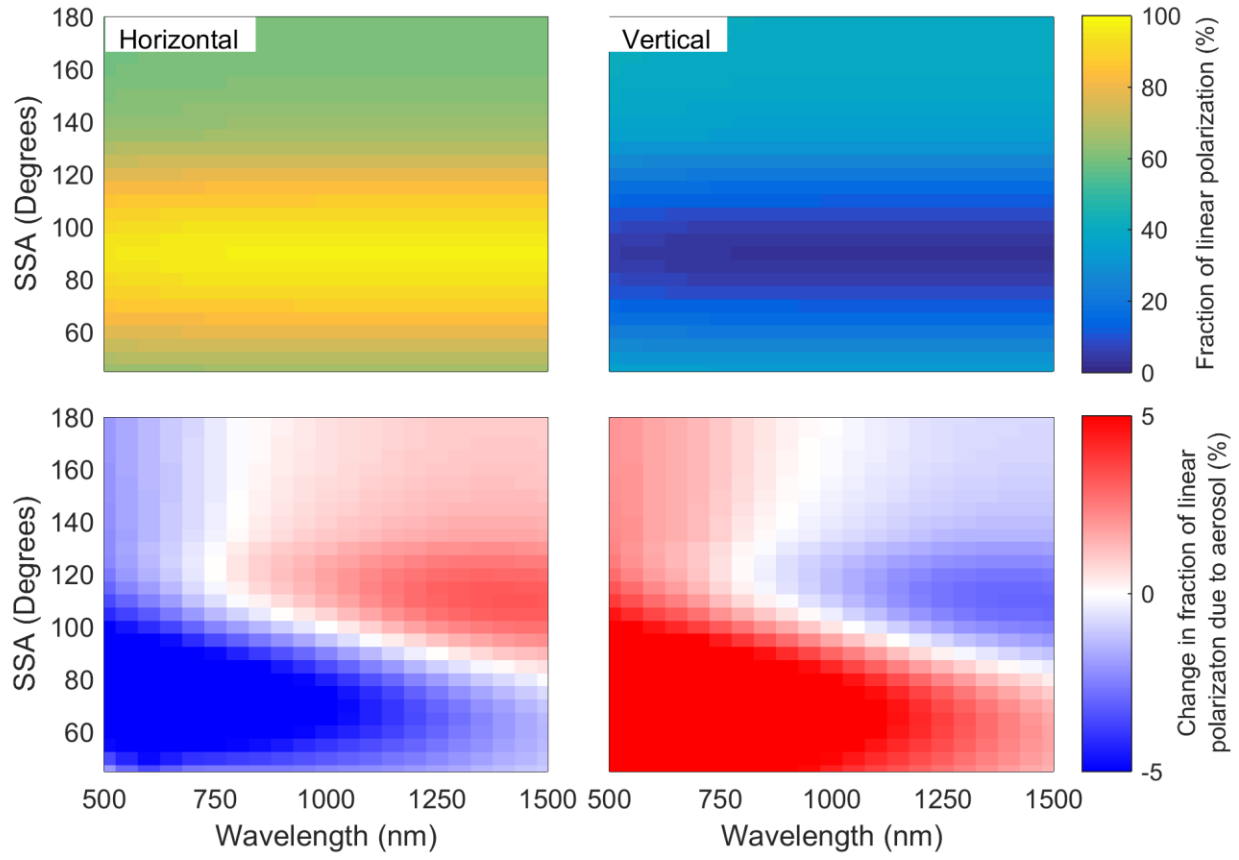

Figure 1: (Top) The fraction of a linear polarization (left is horizontal and right is vertical) over the total radiance for molecular air density. (Bottom) The change in the fraction of linear polarization between an atmosphere that contains aerosol and one with only molecular air density. This data was simulated with SASKTRAN including multiple scattering.

2.2 SASKTRAN-HR model

The High Resolution module of the SASKTRAN radiative transfer framework (Bourassa et al., 2007; Zawada et al., 2015) [14, 28] was used in this study. The SASKTRAN framework handles built-in and user-specified atmospheric species optical properties and number density profiles, and assumes a fully 3D spherical geometry to solve the radiative transfer equation. The High Resolution module uses a successive orders of scattering technique, and solves either the scalar or vector (polarized) radiative transfer equations to arbitrarily many orders of scatter. In this study, the HR module is configured so that for any photon trajectory the first two scattering events in the atmosphere (from the Sun) and the final scattering event into the instrument line of sight are treated in a fully polarized sense; any intervening scattering events treat the photon as randomly polarized. For example: If a photon scatters three times to enter the line of sight, each scattering event is treated in a fully polarized sense; if a photon scatters five times to enter the line of sight, the first two scattering events are polarized, the photon is then depolarized and undergoes two scattering events, and finally undergoes a polarized scattering event from its randomly polarized state into the line of sight. This pseudo-polarized approximation has been shown, through comparison against the highly accurate and fully polarized Monte Carlo module of the SASKTRAN-HR framework (Dueck et al., 2016) [29], to approximate the full solution of the vector radiative transfer equation to sufficient accuracy for the wavelengths and geometries of interest in this work. This pseudo-polarized approximation was used for quicker processing times. All calculations performed with SASKTRAN-HR in this study assume randomly polarized incident sunlight, and dry air and Mie (H_2SO_4) scattering events only to model the interaction with the molecular air density and stratospheric aerosol, respectively. Scattering events from the Earth's surface are assumed to be Lambertian and fully depolarizing. The assumption of a Lambertian surface is commonly used even though in many cases a Lambertian surface does not accurately describe surface polarized scattering (Martonchik et al., 1998; Deuzé et al., 2000) [30, 31].

2.3 Model Scenarios

The impact of using polarized radiance measurements on stratospheric aerosol retrievals is systematically studied with the radiative transfer model by exploring a set of distinct cases that approximately cover the expected range of aerosol parameters, including both particle size and concentration (or extinction) profiles, and viewing geometries. Viewing geometry is an important parameter as even in the case of the total radiance measurements, the geometry can have a substantial effect on the sensitivity of the measurement to aerosol due to the asymmetry of the Mie scattering phase function, i.e. element $P_{11}(\Theta)$ of the scattering matrix (Rieger et al., 2014) [16]. Aerosols scatter strongly in the forward direction resulting in a weaker relative aerosol signal in the back scatter direction.

To probe the space of possible aerosol measurement scenarios, two aerosol extinction coefficient profiles and four particle size distributions were used. The two extinction profiles, nominally specified at 750 nm, correspond to a background aerosol case, typical of the volcanically quiet period of the early 2000's (Deshler et al., 2003) [32], and a volcanically enhanced case which was taken from OSIRIS measurements two months after the Nabro eruption in 2012 (Bourassa et al., 2012c) [33]. Both profiles are shown in Figure 2. The four particle size distributions were also chosen to represent typical background and volcanically enhanced cases. The background cases are both single mode lognormal distributions with somewhat different, but still typically observed, size parameters. A bi-modal lognormal particle size

distribution was used for the volcanically enhanced cases, with one fine mode and one coarse mode, each comprising an equal fraction of the total extinction. All of the parameters of the size distributions are detailed in Table 1. These selected distributions are based on in-situ balloon particle counter measurements from Laramie, Wyoming (Deshler et al., 2003) [32]. The size distributions were used for translating the extinction profiles, which are specified at 750 nm, to other wavelengths by scaling the extinction by the ratio of the Mie scattering cross sections corresponding to the size distribution at the two wavelengths.

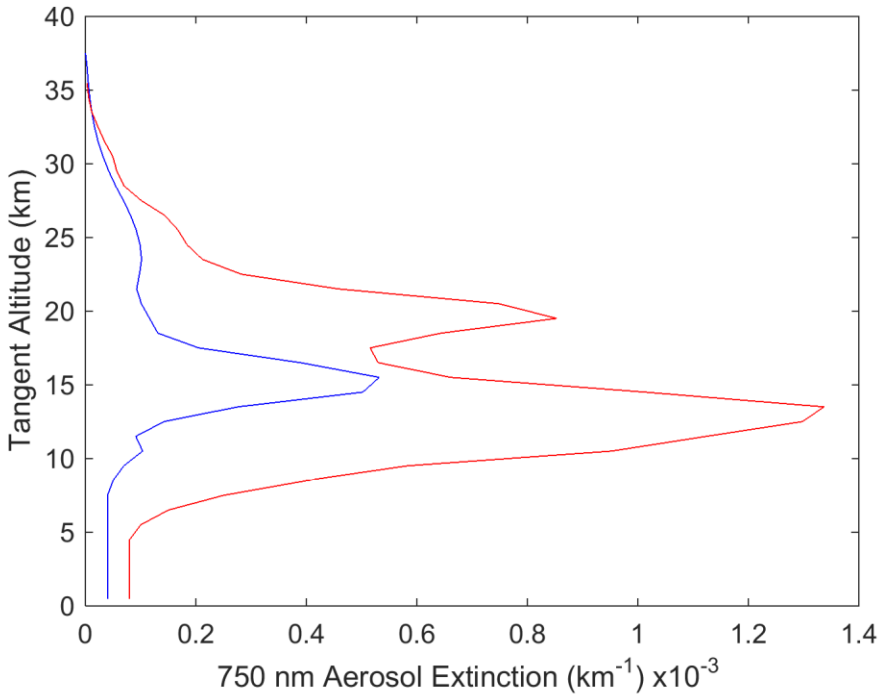

Figure 2: The two aerosol extinction profiles used in this study. The blue profile represents a background aerosol extinction levels, and the red curve is a representative aerosol profile after the Nabro eruption. The aerosol optical depths are 3.9×10^{-3} and 1.335×10^{-2} for the background and Nabro profiles respectively.

Particle size distributions	Fine mode radius (µm)	Fine mode width	Coarse mode radius (µm)	Coarse mode width	Percent extinction coarse mode (%)
1	0.04	1.8	--	--	0
2	0.12	1.25	--	--	0
3	0.04	1.8	0.30	1.15	50
4	0.12	1.25	0.30	1.15	50

Table 1: Different particle size distributions used to test the sensitivity of the aerosol retrieval.

To probe the range of possible viewing geometries from a low earth orbit, a range of Solar Zenith Angles (SZAs) and SSA were selected. The ranges give representative selections of the possible geometries of a limb scatter instrument in low earth orbits at a range of local times. The selected values for SZA are 15 °, 45 °, and 75° and for SSA of 30°, 60°, 90°, 120°, 150°, and 180°.

Simulated measurements were performed at wavelengths of 500, 750, 1000, 1250, and 1500 nm, which approximately covers the spectral range commonly used for aerosol retrievals from limb instruments. For example, OSIRIS and SCHIAMACHY aerosol products use the ratio of 750 nm to 470 nm for the aerosol retrieval (Bourassa et al., 2012b; Ernst et al., 2012) [15, 19]. Additional longer wavelengths have been shown to provide particle size information from limb scatter measurements (Rieger et al., 2014) [16] and so the 1000-1500 nm wavelength range was also included in this study. Finally, we also performed simulations for Earth surface albedo values of 0 and 1 in order to cover the full range of potential impact.

3 Methodology

For the purposes of this study, we have assumed an instrument capable of measuring only the linearly polarized radiance with either a vertical or horizontal orientation. This is representative of newly proposed instruments like ALTIUS (Dekemper et al., 2012; Fussen et al., 2016) [20, 21] and ALI (Elash et al., 2016) [22] that use an acousto-optic tunable filter and by nature only measure one orientation of linearly polarized radiance. We want to answer the question: If the linear polarization is measured, is this an advantage or a disadvantage over a measurement of the total radiance for aerosol retrievals? Further, is there a preferred orientation of linear polarization?

The polarization states used here are defined as follows: the linearly polarized radiance aligned with the horizon is referred to as the horizontal polarization, and the linearly polarized radiance that is perpendicular to the horizon is referred to as the vertical polarization. We also use the total radiance, or alternatively the scalar radiance, as the reference case. Note that the scalar radiance is not precisely equal to the total radiance. For the work presented here the term "total radiance" refers to the first term in the Stokes vector, which is calculated by the SASKTRAN-HR model when solving the vector radiative transfer equation. The term "scalar radiance" refers to the radiance calculated by the SASKTRAN-HR model when solving the scalar transfer equation. Using the Stokes parameter formulation, the horizontal polarization is given by $0.5(I + Q)$ and the vertical polarization is given by $0.5(I - Q)$, which can be easily shown from the definitions given in Equation 2.

Our study further breaks down this problem into three questions. First, how does the fraction of the limb scatter signal that is due to aerosol vary with aerosol load and viewing geometry for both scalar and polarized measurements? Secondly, does the polarized measurement increase sensitivity to assumptions in the retrieval algorithm and therefore increase potential for biased results? And finally, how does the polarized measurement affect the uncertainty estimate of the retrieved profile?

To explore the first question, simulated measurements were calculated with SASKTRAN-HR using the scenarios described in section 2.3, including various wavelengths, geometries, aerosol loading and particle size distributions. These simulated measurements are then used to determine the approximate fraction of the limb signal that is due to aerosol. In each case the model is run with a nominal atmosphere that consists of molecular air density, and climatological ozone and nitrogen dioxide profiles.

The fraction of the limb signal due to aerosol is determined by calculating the radiance without aerosol in the model atmosphere, i.e. that due to Rayleigh scattering only, I_R, and the radiance including aerosol, I_A.

To find the fraction, δ, in percentage, of the signal that is attributed to aerosol, the following formulation is used:

$$\delta = \frac{I_A - I_R}{I_A} * 100\% \quad (6)$$

Due to the non- linear behavior of multiple scattering, it is not strictly true that this is the fraction of the signal due to aerosol; however, at most stratospheric tangent altitudes, the atmosphere is quite optically thin at the considered wavelengths and this simple percent difference provides an intuitive approximation of the fraction of the signal due to aerosol.

We explore the second question about the effect of the polarized measurement on the aerosol retrieval using simulated measurements and a retrieval method that is essentially similar to the one developed by Bourassa et al. (2012b) [15] for OSIRIS. A minor change to the algorithm is made where the measurement vector for this study is not normalized by a shorter wavelength. Although it is advantageous in a retrieval scenario to limit sensitivity to particle size, for this study we explore the worst case scenario under possible limitations of future technology, given that not all instruments may cover a wide enough spectral range for short wavelength normalization.

The limb radiance is calculated using SASKTRAN-HR, again with climatological ozone and NO_2 profiles, for each of the scenarios listed in section 2.3. This is taken as a simulated measurement and is then used to retrieve aerosol extinction profiles using the technique of Bourassa et al., 2012b [15] technique. This is done similarly for the total radiance and for each orientation of the linearly polarized radiance. Additionally, a retrieval is performed with the scalar SASKTRAN-HR model to see if there is any substantial difference between using the scalar radiance and the total radiance from the vector model. For each aerosol retrieval, the ozone, NO_2, and albedo are fixed to the values used in the simulation of the measurement. It should be noted that actual retrieval schemes would need to account for ozone, NO_2, and albedo, which will induce additional uncertainties in the retrieved aerosol extinction profiles. All four particle size distributions from Table 1 are used in the simulations, but following Bourassa et al., 2012b, [15] the aerosol particle size is fixed in the retrieval to a single mode log-normal with 0.08 μm mode radius and mode width of 1.6. The assumption of a fixed particle size distribution is common in limb scatter retrieval algorithms. The difference between the assumed particle size distribution and the true state is used to explore the sensitivity of the retrievals from polarized measurements to the assumed particle size distribution.

Lastly, to answer the third question, an uncertainty estimate is performed on these retrievals in order to check the precision of the retrieved aerosol profile. The precision is determined by mapping the covariance of the measurement vector, S_ϵ through the gain matrix, G, which describes the sensitivity of the retrieval to the measurement and the respective noise through the following equation (Rodgers, 2000) [34]

$$\boldsymbol{S}_{aero} = \boldsymbol{G}\boldsymbol{S}_\epsilon \boldsymbol{G}^T \quad (7)$$

where $\boldsymbol{S}_{aero}$ is the co-variance matrix for the retrieved aerosol profile. However, the direct calculation of the gain matrix is computationally intensive and numerically requires a retrieval for each measured

altitude. A method presented by Bourassa et al. (2012a) [35] uses the Jacobian, $\boldsymbol{K}$, to approximate the gain matrix by assuming the problem is linear near the solution state, which is largely a good assumption for limb scatter aerosol retrievals. Using these assumptions, the gain matrix can be determined simply through the inverse of the Jacobian,

$$\boldsymbol{G} \cong \boldsymbol{K}^{-1}. \quad (8)$$

Rather than specifying an assumed measurement co-variance to study the behavior of the retrieval precision, we simply replace the measurement co-variance in Equation 7 with the identity matrix. Thus the resulting terms of $\boldsymbol{S}_{aero}$ are not absolute quantities but are related to the amplification of the measurement noise when mapped to the retrieved state (i.e. the larger the values of $\boldsymbol{S}_{aero}$ the larger the uncertainty for the retrieval). The square root of the elements of the diagonal of the aerosol covariance, typically used to represent the error bars on the retrieved profile, are taken as the amplification of the measurement noise.

This method assumes that the radiance measurements regardless of polarization state have exactly the same signal to noise performance, i.e. all measurements have the same co-variance. We also consider the case where the instrument is not compensated such that the magnitude of the various polarization states directly scales the signal to noise performance, i.e. the instrument is not compensated to equalize the measurement co-variance when the signal drops due to the measured polarization state. In this scenario the above method must be modified by replacing the identity matrix with the matrix, $\boldsymbol{R}$, to represent the change in signal strength for the various polarizations relative to the scalar case. This matrix is defined as

$$R_{ij} = \begin{cases} \frac{I_{ref,i}}{I_{pol,i}} & \text{for } i = j \\ 0 & \text{for } i \neq j \end{cases}. \quad (9)$$

The diagonal of the $\boldsymbol{R}$ matrix is effectively scaled by the inverse of the magnitude of ratio of the polarized radiance, $I_{pol,i}$, to the reference scalar case, $I_{ref,i}$, for the measurement altitude, i.

4 Analysis

4.1 Difference in Scalar Retrievals Using a Scalar or Vector Model

First, we investigate if there is any significant difference between the use of the scalar radiance and the total radiance for retrievals on measurements of the total radiance. As mentioned above, retrieval algorithms for current limb scatter data sets such as OSIRIS and SCIAMACHY use a scalar radiative transfer model with general success; however, as the total radiance is not generally equal to the scalar radiance, this may lead to biases in the retrieved extinction profile under certain scenarios. Accounting for the vector component in the model alters the overall total radiance from the scalar solution due to multiple scattering interactions between the various polarization states of each successive order of scattering.

The total radiance was simulated with SASKTRAN-HR in vector mode for the full set of wavelengths and viewing geometries, and for the range of aerosol loading scenarios. These were used as input measurements for the retrieval, which was then performed using both the scalar and vector models. A case-by-case comparison between the retrieved extinctions for the scalar and vector models was

performed by calculating simple percentage differences at each retrieval altitude. These have been shown as grey lines in Figure 3. Furthermore, the mean of the bias for each particle size distribution is shown in solid black. These results show that across all wavelengths, the mean percent difference is less than 2% from 15 to 37 km. It should be noted that some of the differences between the two models are removed due to the high altitude normalization in the retrieval measurement vector. A small number of outlier cases occur where the difference between the retrievals is greater than 7%. All of these cases occur for back scatter geometries and short wavelengths. The reason for this discrepancy is not well understood, although it certainly arises from the differences between the scalar and total radiance due to polarization interactions from the relatively larger contribution of multiply scattered light at shorter wavelengths. These discrepancies are enhanced by the reduced sensitivity to aerosol in the back scatter geometries. Generally, however, any differences between the use of the scalar and vector model for the retrieval are negligible. In fact, any form of discrepancy essentially vanishes for wavelengths past 1000 nm. Since the use of the vector model can increase calculation times by a factor of at least two, it is certainly justifiable to use the scalar model for the overwhelming majority of scenarios. For the other cases presented here any reference to the radiance will only refer to the total radiance, I, from the vector model.

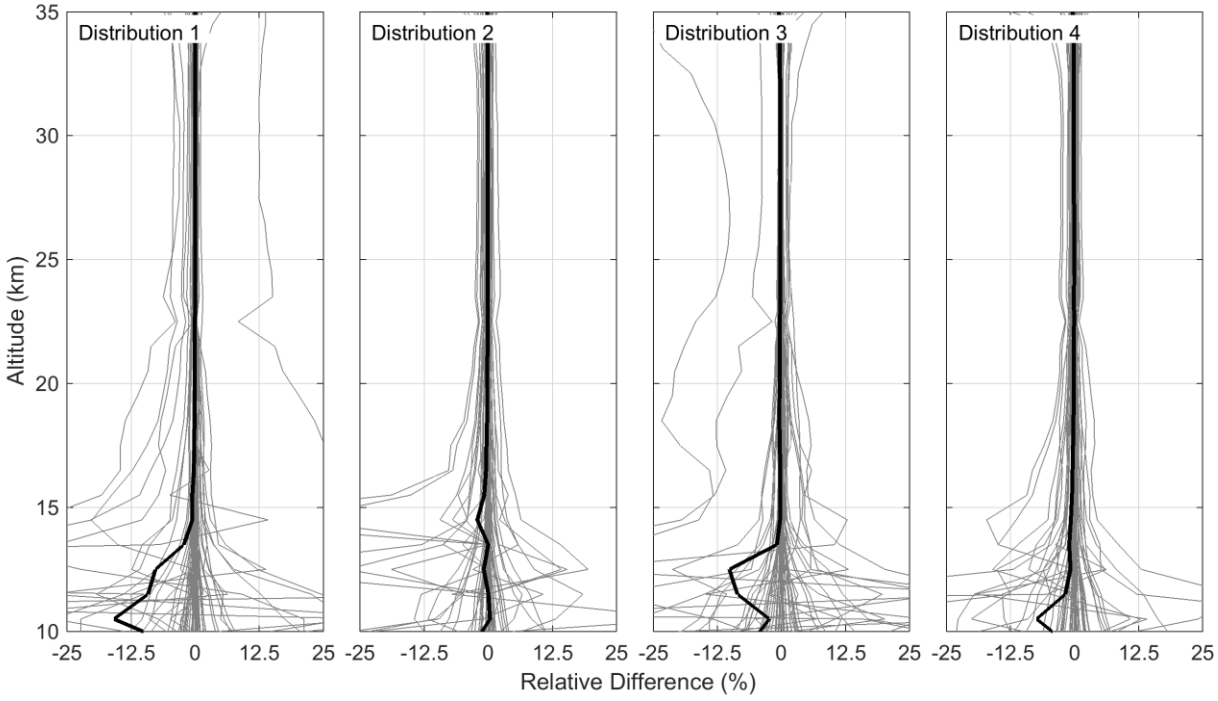

Figure 3: Percent differences between the vector retrieved aerosol extinction profiles and the scalar retrieval from simulated total radiance measurements. Each panel represents a different particle size distribution (see Table 1). The grey lines are the differences for each individual case and the black line is the mean of the bias.

4.2 Fraction of Limb Signal due to Aerosol

For a typical background aerosol state, the fractional contribution to the total limb radiance from aerosol was calculated from modelled radiances over a series of stratospheric tangent altitudes using the background aerosol profile and particle size distribution 1, given in Table 1. Figure 4 shows the percent change in this fraction for horizontally and vertically polarized measurements compared to the total

radiance. The viewing geometry, which is typical for a low earth orbit scenario, is given by SZA=45° and SSA=60°, and the albedo is set to 0 to remove depolarization from the Lambertian Earth. The top of Figure 4 shows the percentage of signal that is attributed to aerosol for both horizontal and vertical linear polarizations, δ, as shown in Equation 6. As can be seen from the bottom of Figure 4, most of the change in the aerosol fraction of the polarized limb signal compared to the total radiance (i.e. $\Delta\,\delta = \delta_{tot} - \delta_{pol}$) occurs for wavelengths between 500-1000 nm, where δ_{tot} and δ_{pol} are the percent aerosol signal as calculated using Equation 6 for the total and a polarized radiance respectively. At these wavelengths the horizontal polarization has a smaller fraction of signal due to aerosol and the vertical polarization has a larger fraction due to aerosol. Overall the change is small and essentially limited to less than 10%.

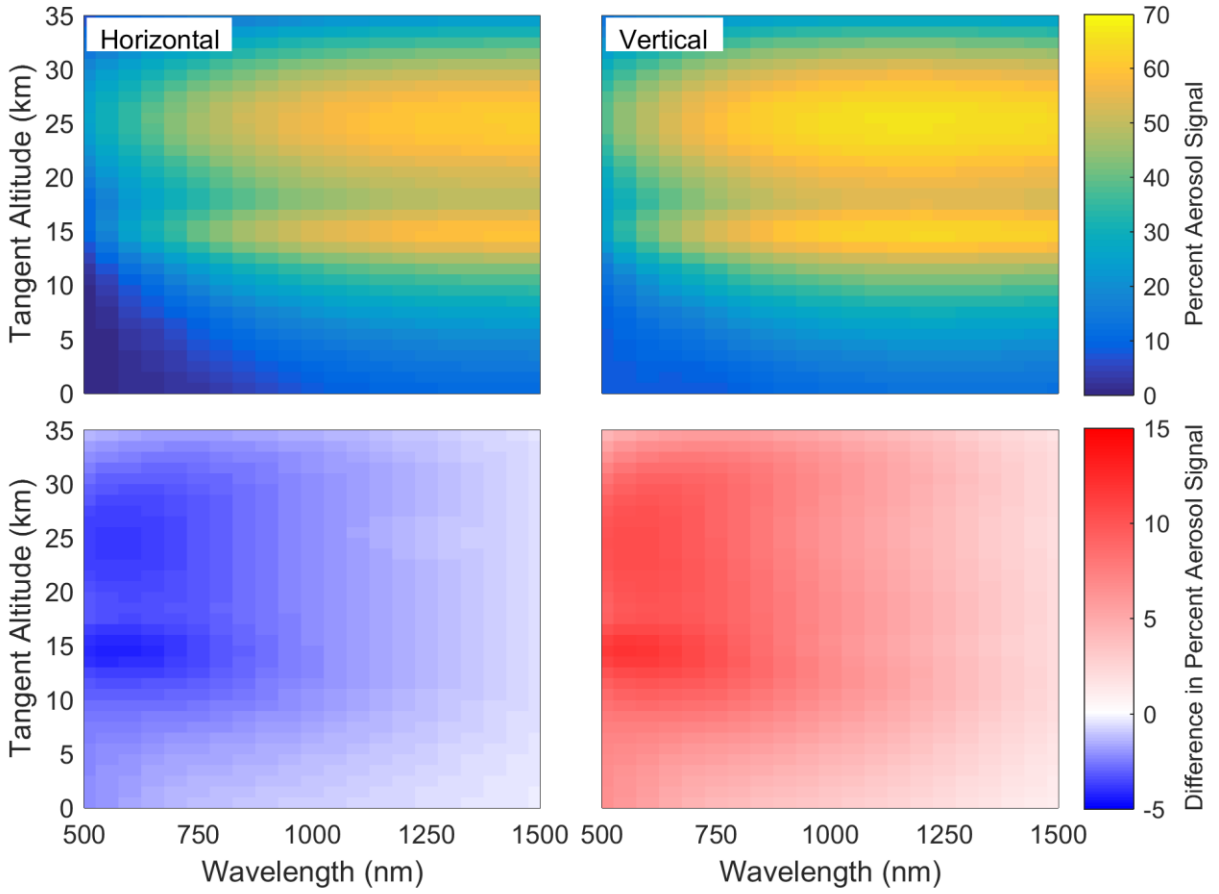

Figure 4: (Top) For a horizontal (left) or vertical (right) linear polarization the percent of the signal that is attributed to aerosol, δ. (Bottom) The change in the fraction of the limb signal due to aerosol when compared to the total radiance for the horizontal (left) and vertical (right) polarization ($\Delta\,\delta$). The simulation uses a geometry of SZA=45° and SSA=60°, with the albedo being 0 and the aerosol state the background profile with particle size distribution 1. Notice that the red-blue scale is asymmetric.

Similar calculations were performed for the range of viewing geometries using the same atmospheric state. Figure 5 shows the fraction of limb signal due to aerosol for the total radiance, and both orientations of the linearly polarized radiance. This calculation was performed for 15 km tangent altitude, and other stratospheric tangent altitudes show very similar patterns. An important difference is noted between the

forward and back scattering geometries. Remembering the horizontal polarization is given by $0.5(I+Q)$, the total and horizontal polarization cases have a similar dependence on viewing geometry, with the strongest aerosol signal from long wavelengths in the forward scatter direction. The vertical polarization, given by $0.5(I-Q)$, has a strong aerosol signal contribution for forward scattering directions, especially at visible wavelengths, in comparison to the total and horizontal polarization cases. For back scattering geometries, somewhat less aerosol signal is observed. For reference, the magnitude of the limb radiance in each case is shown in the right hand column of Figure 5 taking note that the high end of the scale is saturated to emphasise the smaller values. It is important to note that the vertical polarization has a very low magnitude at scattering angles near 90 degrees, making vertically polarized measurements in this geometry particularly susceptible to signal-to-noise problems.

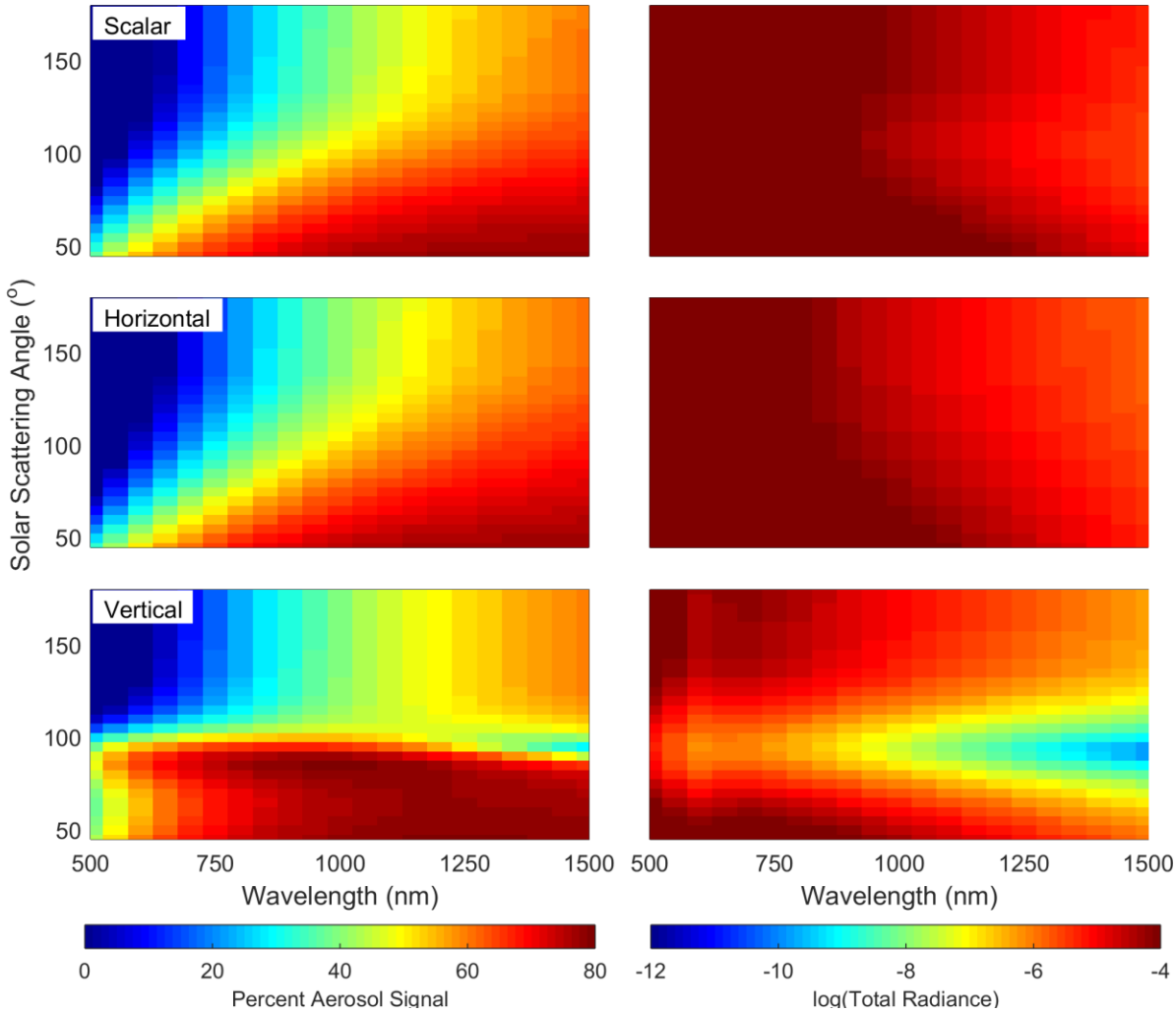

Figure 5: Dependence of the fraction of the limb spectra at 15 km due to aerosol on solar scattering angle (left panels) for total radiance (top), horizontal polarization (middle) and vertical polarization (bottom), and the magnitude of the radiance for each case (right panels). Note the low signal near SSA of 90 degrees for the vertical polarization which would be problematic for terminator orbits.

These same calculations were performed for the full range of SZAs. We found that the SZA affects the fraction of the signal due to aerosol by only less than 1%. Also, when the albedo is changed from 0 to 1, the aerosol signal decreases for all polarizations and wavelengths thus reducing overall sensitivity to aerosol as albedo increases in all cases. Note, however, that the SASKTRAN-HR model assumes that all ground reflection is randomly polarized; the addition of a polarized bidirectional reflectance distribution model may change the sensitivity to aerosol with higher albedo.

This same analysis was also performed for two other additional polarization orientations, the +45 degree and -45 degree linear polarizations (i.e $0.5(I+U)$ and $0.5(I-U)$) to investigate sensitivity to aerosol. It was found that these two polarization orientations had a similar aerosol contribution to the total radiance case with approximately two thirds of the overall signal when compared to the total radiance case.

In general, the contribution to the limb radiance from aerosol for the horizontally polarized and total radiance cases is approximately the same. The vertical polarization has more asymmetry in aerosol signal between forward and back scattering geometries with very low signal magnitude near the scattering angle of 90°. Given that essentially all low earth orbit scenarios will cover forward and backward scattering angles, including the 90° scattering angle, it is clear that the horizontal orientation overall shows a more favorable response to aerosol. This is particularly true for a terminator orbit such as that for OSIRIS.

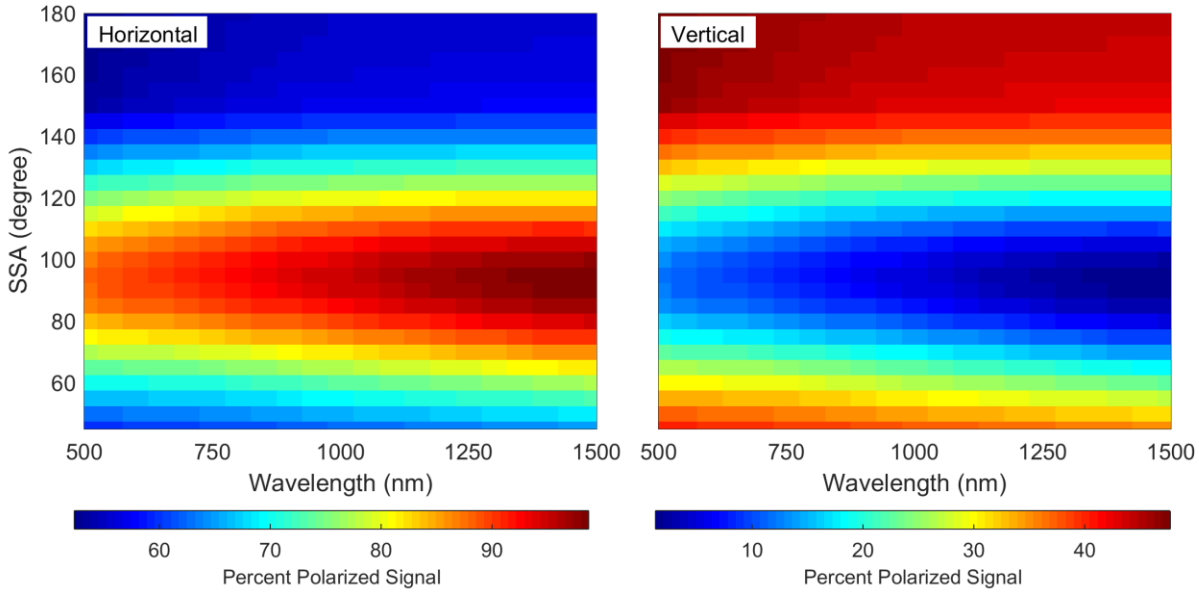

Figure 6: The ratio of the linearly polarized radiance to the total radiance for horizontal (left) and vertical (right) orientations. Note that the scale for each plot is different. The simulation was performed with a SZA of 60 degrees with volcanic aerosol loading for a tangent altitude of 20 km.

A distinct disadvantage of measuring a linear polarization rather than the total radiance is the loss of overall signal magnitude. In Figure 6, the ratio of the polarized radiance to the total radiance is shown for a series of SSAs and a tangent altitude of 20 km, but in this case using the volcanic aerosol extinction profile, which serves to enhance the fraction of signal due to aerosol. Measuring the horizontal polarization results in observing signal levels approximately one half to two thirds of the total radiance, with the greatest signal reduction at the shorter wavelengths. The other forward scatter geometries are

similarly affected. For back scatter geometries, the signal levels are also approximately half of the total radiance, but with less spectral dependence. For SSAs near 90°, the horizontal polarization encompasses a large fraction of the total radiance resulting in signals of 80-95% of the total. Across the full parameter space of viewing geometries, wavelengths, and aerosol loading scenarios, the magnitude of the horizontal polarization is on average 60-70% of the total radiance.

Although the vertical polarization shows a relatively larger fraction of the signal due to aerosol particularly in forward scatter geometries, the overall signal levels are substantially lower. For forward scatter geometries, the magnitude of the vertically polarized radiance is only approximately one third of the total radiance across the spectral range. Back scatter geometries are marginally better with slightly less than half of the total radiance. Again, near SSAs of 90° the limb radiance is almost fully horizontally polarized and the vertically polarized signal is only 5-20% of the total. On average across the entire parameter space, the vertical polarization component typically accounts for 30-40% of the total signal.

It is clear from this relatively simplistic analysis of the aerosol signal in polarized limb radiance that there are trade-offs between viewing geometries and instrument polarization sensitivity, and changing sensitivity across the spectral range. While there is not an overwhelming case to be made for one particular option over the wide range of scenarios that can be considered, the overall response of the horizontally polarized radiance is essentially similar to the total radiance, but with somewhat reduced magnitude that can most likely be mitigated through instrument design considerations. The vertical polarization has much more widely varying sensitivity to aerosol with very low signal levels near 90 degrees scattering angle, and is a much more challenging choice in terms of instrument performance for aerosol measurements.

4.3 Potential for Retrieval Bias

In this section we directly explore the effect of the polarized measurement on the results of a typical retrieval algorithm through application of the algorithm to simulated measurements across the full parameter space.

We explore the potential of an effect of polarization on the bias in retrieved extinction caused by uncertainty in the assumed particle size distribution. The set of radiances for all cases across the parameter space were again used as simulated input measurements to the retrieval algorithm. This time, retrievals were performed on the horizontally polarized radiance, the vertically polarized radiance, and the total radiance. The model calculations in the retrieval algorithm were set to match the polarization state of the input radiance. Note that total radiance is used from the vector SASKRAN-HR model for the total radiance case. In all cases, the retrieval was performed assuming a fixed log-normal particle size distribution with a mode radius and width of 0.08 μm and 1.6 respectively. Note that this assumed size distribution is different than all four of the size distributions used as the “true” state for the simulated input radiances. For the total radiance case, this uncertainty is well known to cause biases of up to 20-30% in retrieved extinction (Rieger et al., 2014) [16]. A summary of the differences between the retrieved and true aerosol extinction for 750 nm and 20 km altitude is shown in Figure 7 and is similar for altitudes from 17 to 35 km. Errors bars on each point represent one standard deviation of the variability in the results for the range of viewing geometries. These results are representative of the level of agreement also found for other wavelengths and altitudes. There is no substantial difference between the absolute

magnitude of the bias for the background and volcanic extinction profiles, but the difference in sign of the bias is expected. It should be noted that cases with SSA of 90° have been removed for the vertical polarization due to the very low values of signal, which manifests as a large dependency on the particle size distribution and a highly biased retrieval. This large bias rapidly disappears for SSAs farther away from 90° and is almost gone for SSAs of 85° or 95°.

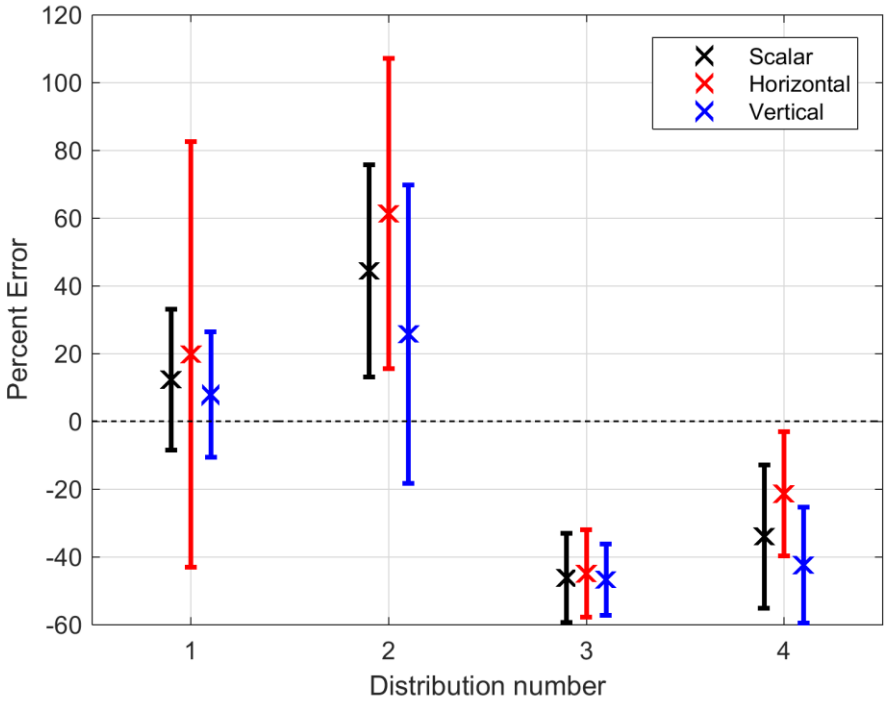

Figure 7: The mean percent difference between the retrieved aerosol extinction profile with an assumed particle size distribution and the true state corresponding to the indicated particle size distribution (see Table 1). Error bars represent one standard deviation of the variability across all viewing geometries. Results shown are for 750 nm and 20 km altitude.

It is clear that the major element of observed bias is simply due to the difference between the true and assumed particle size distribution. In all four cases there is some difference between the solutions for the various polarization states; however, for each particle size distribution the biases between the polarization states are essentially the same within the variability observed across the various viewing geometries. None of the linearly polarized states perform consistently better than the total radiance case; however, they do not perform any worse either (excepting the vertical polarization near 90 degree SSA), which is an equally important result.

4.4 Precision Analysis

Finally, we study the effect of the polarized measurement on the performance of the retrieval in terms of the precision of the results. We again use simulated measurements across the full range of input parameters as input to the standard retrieval algorithm. Following the methodology outlined in Section 3, using SASKTRAN-HR the Jacobian matrices were calculated for each retrieved state and used to determine the gain matrices, which were then applied as in Equation 7 to determine the retrieval precision. It should be noted that not all of the Jacobian matrices could be inverted due to small sensitivity

at the lower tangent altitudes (see discussion in Bourassa et al., 2007) [14] and these were removed from the data set (approximately 9% of all cases). This affected a large fraction of the 500 nm cases, so this wavelength was removed from this section of the analysis. As discussed in Section 3, we approach this problem from two perspectives: (1) an instrument that is compensated in design and/or operation such that measurements regardless of polarization state or geometries have the same signal to noise ratio, and (2) an uncompensated instrument such that the changing signal level with polarization state and viewing geometry affects the signal to noise ratio of the observation.

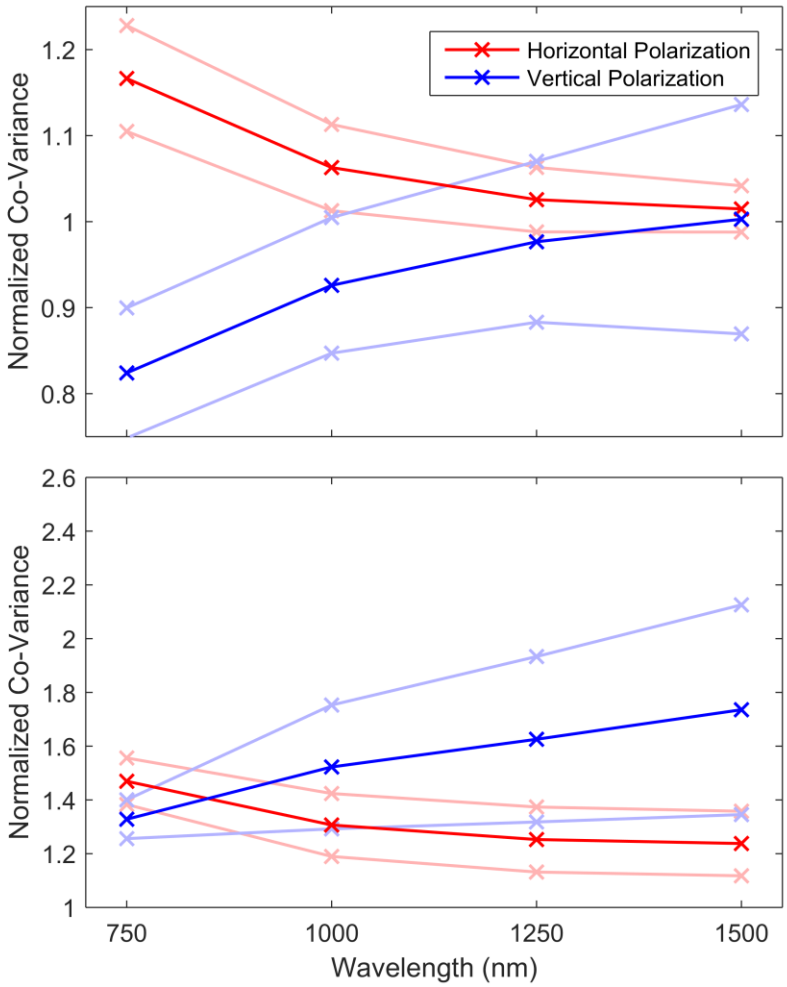

Figure 8: The wavelength dependence of the co-variance for the horizontal and vertical polarization retrievals normalized to the total radiance case. The faded line represent one standard deviation of the variability encountered across all input parameters. The top panel is for an instrument design and/or operation that compensates for changing signal levels with polarization and viewing geometry, and the bottom panel is for uncompensated measurements.

For the compensated case, the measurement co-variance matrix in Equation 7 is replaced with the identity matrix, and the relative size of the square root of the diagonal of the resulting aerosol co-variance represents the amplification of the measurement noise. To compare the performance of the various polarization states, the resulting retrieval co-variances for the linearly polarized measurements were

normalized by the retrieval co-variances from the total radiance case. The dependence of the results on the various input parameters, such as wavelength and viewing geometry were examined. Very little altitude dependence was observed and so the results were averaged across the retrieved altitude range.

In Figure 8 the normalized co-variances cases were sorted by wavelength using all geometries and atmospheric states. These bins were then averaged for each wavelength shown by the red and blue points for the horizontal and vertical polarization respectively. The fainted colours represent one standard deviation around the mean. Each of the means in Figure 8 contains between 186 to 229 unique data points. Values smaller or larger than one respectively indicate retrieval uncertainties smaller or larger than the total radiance retrieval uncertainties.

The resulting normalized co-variances have a substantial dependence on wavelength. The situation where the signal to noise ratio is compensated such that it is equal for all cases is shown in the top panel of Figure 8, where the vertical polarization has a smaller co-variance, i.e. better precision, by approximately 20% at the shorter wavelengths than the total radiance retrieval. As wavelength increases to 1500 nm, the precision of the vertical polarization case is approximately equal to that of the total radiance case. The horizontal polarization essentially mirrors the vertical case with higher co-variances than total radiance at short wavelengths and approximately equal at 1500 nm. Recall, however, that the vertical polarization has significantly lower signal levels and in order for the measurement to be compensated to obtain equal signal to noise levels, an increase in instrument sensitivity or exposure time would be required.

Across the range of SSAs, the vertical polarization has slightly lower co-variance than the other two cases, except at 90 degrees, which is due to the lack of sensitivity in this region noted previously. Table 2 shows the calculated means and standard deviations across SSA for the horizontal and vertical polarizations. Note that SSA of 90^o is missing due to the poor signal, and the associated high retrieval co-variances for this geometry. Furthermore, the variability of the result across all of the other input parameters increases dramatically as the scattering angle approaches 90 degrees. The precision of the retrieval shows very little dependence on the other input parameters such as solar zenith angle, albedo, particle size distribution, and extinction level. On average across all parameters, the retrieved co-variance from the vertical polarization is approximately 15% smaller than the horizontally polarized retrieval.

Polarization	60^o	90^o	120^o	150^o	180^o
Horizontal (Compensated)	1.072±0.051	1.090±0.082	1.047±0.078	1.027±0.048	1.023±0.042
Vertical (Compensated)	0.861±0.084	--	0.968±0.157	0.977±0.063	0.980±0.051
Horizontal (Uncompensated)	1.289±0.075	1.225±0.158	1.261±0.165	1.341±0.098	1.360±0.085
Vertical (Uncompensated)	1.576±0.167	--	1.852±0.559	1.527±0.170	1.490±0.130

Table 2: The SSA dependence of the normalized co-variance for the horizontal and vertical polarization retrievals. The given numbers are the mean with the standard deviation for each geometry across all wavelengths. Note that the SSA of 90^o for the vertical polarization has been removed due to the poor signal in this region.

In the case of an uncompensated instrument, for example where a linear polarizer is added to the optical chain with no other changes in observation, the scaling of the diagonal of the measurement co-variance is used as outlined in section 3. Due to the larger magnitude of the signal in the horizontal polarization compared to the vertical polarization, the horizontal cases generally have lower retrieval co-variance, and this effect increases with longer wavelength as seen in the lower panel of figure 8. Note that in this uncompensated case, since the linear polarizations are always some fraction of the total radiance, the co-

variance is always larger than the total radiance case (i.e. the normalized co-variances are always greater than 1). Once again very little dependence on solar zenith angle, albedo, size distribution or extinction level was observed. There was also little dependence on SSA, except for vertical polarization at 90 degrees. On average across all parameters, vertical and horizontal polarizations have approximately a 60% and 30% larger uncertainty than the total radiance case, respectively.

This analysis shows that the main driver of retrieval precision is the signal to noise level of the observation, as would be expected. Again, this leads to instrument design and/or operational considerations in order to maintain retrieval precision at the same level as the total radiance measurement. A main scientific goal of both the ALI and ALTIUS instruments is obtaining high spatial resolution observations, both vertically and horizontally along, and across, the satellite track. This generally means that images must be collected rapidly and long exposure times are not an affordable luxury. Once more, the relatively higher magnitude signal levels of the horizontal polarization point to this as the more appealing choice of orientation; however, compared to the total radiance case the decreased precision is larger for the horizontal polarization at shorter wavelengths.

5. Conclusions

We have attempted to address the question of whether or not the measurement of linearly polarized radiance rather than total limb radiance represents an advantage or disadvantage with respect to retrievals of stratospheric aerosol. The sensitivity of the polarized limb radiance to aerosol is a complicated function with respect to many parameters, and there are trade-offs in the orientation of the polarization and the orbital viewing geometry. One important point is the very low magnitude of signal observed in the vertical polarization for scattering angles near 90 degrees, which are encountered for a large fraction of observations in low earth orbit, particularly sun-synchronous near-terminator orbits such as for OSIRIS. More generally, it is important to consider the overall lower magnitude of the linearly polarized radiance, which by definition is a fraction of the total radiance. The horizontal polarization has, on average, higher signal levels than the vertical polarization. It also has a weaker dependence on SSA that is more similar to the total radiance than the vertical polarization, which is more strongly skewed in the forward scatter direction.

One critical bias in limb scatter retrievals of stratospheric aerosol is caused by the uncertainty in the assumed particle size parameters. We tested four different particle size distribution scenarios, representing background and volcanically perturbed conditions, over a large range of other parameters such as wavelength, viewing geometry, and extinction level and found that there is no significant change in the observed bias for polarized or total radiance measurements. So, with respect to this bias in stratospheric aerosol retrievals, the linearly-polarized measurement can be used to achieve approximately equal results with only minor advantages and disadvantages between the different polarization states.

The polarized measurement can have an effect on the precision of the retrieval, where again the main driver is the magnitude of the signal. For a compensated instrument, the polarization can either increase or decrease the precision and there is an apparent trade-off between signal levels and performance of the vertical or horizontal polarization. This is mostly important at shorter wavelengths since at longer wavelengths the differences are negligible. For an uncompensated instrument, the precision of the

retrieved aerosol extinction from a polarized measurement is always inferior to the total radiance case. However the horizontal polarization has better signal levels thus yielding more precise results.

In conclusion, we have found no clear advantage to the linearly polarized measurement over the total radiance for aerosol retrievals; however, there are also no clear disadvantages assuming the somewhat lower overall signal levels can be handled in the instrument design or operation. With careful choice of the orientation of the measured polarization with respect to the orbital geometry and desired coverage, an instrument such as ALI or ALTIUS is fully capable of obtaining retrieved aerosol products of very similar quality compared to an equivalent instrument that measures the total radiance.

Acknowledgements

This work would have not been possible without funding from Natural Sciences and Engineering Research Council (Canada) and the Canadian Space Agency's FAST program. Thanks to Nick Lloyd for assistance and guidance in the use of the SASKTRAN-HR model.

References

[1] Kiehl, J. T., and B. P. Briegleb (1993), The relative roles of sulfate aerosols and greenhouse gases in climate forcing, Science, 260, 311-314, doi:10.1126/science.260.5106.311.

[2] Stocker, T. F., D. Qin, G.-K. Plattner, M. M. Tignor, S. K. Allen, J. Boschung, A. Nauels, Y. Xia, V. Bex, and P. M. Midgley (2013), Climate Change 2013 The Physical Science Basis.

[3] Solomon, S., J. S. Daniel, R. R. Neely, J.-P. Vernier, E. G. Dutton, and L. W. Thomason (2011), The persistently variable background stratospheric aerosol layer and global climate change, Science, 333, 866-870, doi:10.1126/science.1206027.

[4] Haywood, J. M., A. Jones, and G. S. Jones (2014), The impact of volcanic eruptions in the period 2000-2013 on global mean temperature trends evaluated in the HadGEM2-ES climate model, Atmospheric Science Letters, 15, 92-96, doi:10.1002/asl2.471.

[5] Fyfe, J. C., N. P. Gillett, and F. W. Zwiers (2013), Overestimated global warming over the past 20 years, Nature Climate Change, 3, 767-769.

[6] Vernier, J.-P., Thomason, L. W., Pommereau, J.-P., Bourassa, A., Pelon, J., Garnier, A., Hauchecorne, A., Blanot, L., Trepte, C., Degenstein, D., and Vargas, F. (2011), Major influence of tropical volcanic eruptions on the stratospheric aerosol layer during the last decade, Geophys. Res. Lett., 38, L12807, doi:10.1029/2011GL047563.

[7] Neely, R. R., Yu, P., Rosenlof, K. H., Toon, O. B., Daniel, J. S., Solomon, S., and Miller, H. L.(2014), The contribution of anthropogenic SO2 emissions to the Asian tropopause aerosol layer, J. Geophys. Res., 119, 1571–1579, doi:10.1002/2013JD020578.

[8] Kremser, S., L. W. Thomason, M. von Hobe, M. Hermann, T. Deshler, C. Timmreck, M. Toohey, A. Stenke, J. P. Schwarz, R. Weigel, S. Fueglistaler, F. J. Prata, J.-P. Vernier, H. Schlager, J. E. Barnes, J.-C. Antuña-Marrero, D. Fairlie, M. Palm, E. Mahieu, J. Notholt, M. Rex, C. Bingen, F. Vanhellemont, A. Bourassa, J. M. C. Plane, D. Klocke, S. A. Carn, L. Clarisse, T. Trickl, R. Neely, A. D. James, L. Rieger, J. C. Wilson, and B. Meland (2015), Stratospheric aerosol—Observations, processes, and impact on climate, Rev. Geophys, 54, doi:10.1002/2015RG000511.

[9] Russell, P., and M. McCormick (1989), SAGE II aerosol data validation and initial data use: An introduction and overview, Journal of Geophysical Research: Atmospheres (1984-2012), 94, 8335-8338.

[10] Thomason, L. W., and G. Taha (2003), SAGE III aerosol extinction measurements: Initial results, Geophysical research letters, 30.

[11] Llewellyn, E., N. D. Lloyd, D. A. Degenstein, R. L. Gattinger, S. V. Petelina, A. E. Bourassa,J. T. Wiensz, E. V. Ivanov, I. C. McDade, B. H. Solheim, J. C. McConnell, C. S. Haley,C. von Savigny, C. E. Sioris, C. A. McLinden, E. Grifoen, J. Kaminski, W. F. J. Evans, E. Puckrin, K. Strong, V. Wehrle, R. H. Hum, D. J. W. Kendall, J. Matsushita, D. P. Murtagh, S. Brohede, J. Stegman, G. Witt, G. Barnes, W. F. Payne, L. Piche, K. Smith, G. Warshaw, D. L. Deslauniers, P. Marchand, E. H. Richardson, R. A. King, I. Wevers, W. McCreath, E. Kyrola, L. Oikarinen, G. W. Leppelmeier, H. Auvinen, G. Megie, A. Hauchecorne, F. Lefevre, J. de La Noe, P. Ricaud, U. Frisk, F. Sjoberg, F. von Scheele, and L. Nordh (2004), The OSIRIS instrument on the Odin spacecraft, Canadian Journal of Physics, 82, 411-422, doi:10.1139/p04-005.

[12] Bovensmann, H., J. Burrows, M. Buchwitz, J. Frerick, S. Noël, V. Rozanov, K. Chance, and A. Goede (1999), SCIAMACHY: Mission objectives and measurement modes, Journal of the Atmospheric Sciences, 56, 127-150.

[13] Rault, D. F., and R. P. Loughman (2013), The OMPS limb profiler environmental data record algorithm theoretical basis document and expected performance, Geoscience and Remote Sensing, IEEE Transactions on, 51, 2505-2527.

[14] Bourassa, A. E., D. A. Degenstein, R. L. Gattinger, and E. J. Llewellyn (2007), Stratospheric aerosol retrieval with optical spectrograph and infrared imaging system limb scatter measurements, Journal of Geophysical Research, 112, D10217, doi:10.1029/2006JD008079.

[15] Bourassa, A. E., L. A. Rieger, N. D. Lloyd, and D. A. Degenstein (2012b), Odin-OSIRIS stratospheric aerosol data product and SAGE III intercomparison, Atmospheric Chemistry & Physics, 12, 605-614, doi:10.5194/acp-12-605-2012.

[16] Rieger, L. A., A. E. Bourassa, and D. A. Degenstein (2014), Stratospheric aerosol particle size information in Odin-OSIRIS limb scatter spectra, Atmospheric Measurement Techniques, 7, 507-522, doi:10.5194/amt-7-507-2014.

[17] Rieger, L. A., A. E. Bourassa, and D. A. Degenstein (2015), Merging the OSIRIS and SAGE II stratospheric aerosol records, Journal of Geophysical Research: Atmospheres, doi:10.1002/2015JD023133, 2015JD023133.

[18] Thomason et al., in preparation

[19] Ernst, F., C. von Savigny, A. Rozanov, V. Rozanov, K.-U. Eichmann, L. A. Brinkho, H. Bovensmann, and J. P. Burrows (2012), Global stratospheric aerosol extinction profile retrievals from SCIAMACHY limb-scatter observations, Atmospheric Measurement Techniques, 5, 5993-6035, doi:10.5194/amtd-5-5993-2012.

[20] Dekemper, E., N. Loodts, B. V. Opstal, J. Maes, F. Vanhellemont, N. Mateshvili, G. Franssens, D. Pieroux, C. Bingen, C. Robert, L. D. Vos, L. Aballea, and D. Fussen (2012), Tunable acousto-optic spectral imager for atmospheric composition measurements in the visible spectral domain, Applied Optics, 51, 6259-6267, doi:10.1364/AO.51.006259.

[21] Fussen, D., E. Dekemper, Q. Errera, G. Franssens, N. Mateshvili, D. Pieroux, and F. Vanhellemont (2016), The ALTIUS mission, Atmospheric Measurements Techniques Discussions, doi:10.5194/amt-2016-213, in review.

[22] Elash, B. J., A. E. Bourassa, P. R. Loewen, N. D. Lloyd, and D. A. Degenstein (2016), The Aerosol Limb Imager: Acousto-Optic Imaging of Limb Scattered Sunlight for Stratospheric Aerosol Profiling, Atmospheric Measurement Techniques, 9, 1261-1277, doi:10.5194/amt-9-1261-2016.

[23] McLinden, C. A., J. C. McConnell, C. T. McElroy, and E. Griffioen (1999), Observations of Stratospheric Aerosol Using CPFM Polarized Limb Radiances, Journal of the Atmospheric Sciences 1999 56:2, 233-240, doi:10.1175/1520-0469(1999)056<0233:OOSAUC>2.0.CO;2.

[24] Mishchenko, M. I., L. D. Travis, and A. A. Lacis (2002), Scattering, Absorption, and Emission of Light by Small Particles, 3rd edition, Cambridge, UK: Cambridge University Press.

[25] Van de Hulst, H. C. (1962), Light Scattering by Small Particles, New York: Wiley and Sons Inc.

[26] Mie, G. (1908), Considerations on the optics of turbid media, especially colloidal metal solutions, Ann. Phys. (Leipzig)., 42, 377.

[27] Wiscombe, W. J.: Improved mie scattering algorithms, Appl. Optics, 19, 1505–1509, 1980.

[28] Zawada, D. J., S. R. Dueck, L. A. Rieger, A. E. Bourassa, N. D. Lloyd, and D. A. Degenstein (2015), High resolution and Monte Carlo additions to the SASKTRAN radiative transfer model, Atmospheric Measurement Techniques, 8, 3357-3397, doi:10.5194/amtd-8-3357-2015.

[29] Dueck, S., A. E., Bourassa, and D. A. Degenstein (2016), Polarization Additions SASKTRAN Radiative Transfer Model, In Preparations.

[30] Deuzé, J. L., P. Goloub, M. Herman, A. Marchand, G. Perry, S. Susana, and D. Tanré (2000), Estimate of the aerosol properties over the ocean with POLDER, Journal Geophysical Research, 105(D12), 15329–15346, doi:10.1029/2000JD900148.

[31] Martonchik J. V., D. J. Diner, R. A. Kahn, T. P. Ackerman, M. M. Verstraete, B. Pinty, and H. R. Gordon, Techniques for the retrieval of aerosol properties over land and ocean using multiangle imaging, IEEE Transactions on Geoscience and Remote Sensing, 36- 4, 1212-1227, doi: 10.1109/36.701027.

[32] Deshler, T., M. Hervig, D. Hofmann, J. Rosen, and J. Liley (2003), Thirty years of in situ stratospheric aerosol size distribution measurements from Laramie, Wyoming (41 N), using balloon-borne instruments, Journal of Geophysical Research: Atmospheres (1984-2012), 108.

[33] Bourassa, A. E., A. Robock,W. J. Randel, T. Deshler, L. A. Rieger, N. D. Lloyd, E. T. Llewellyn, and D. A. Degenstein (2012c), Large volcanic aerosol load in the stratosphere linked to Asian monsoon transport, Science, 337, 78–81.

[34] Rodgers, C. (2000), Inverse Methods for Atmospheric Sounding: Theory and Practice, Series on atmospheric, oceanic and planetary physics: 1999, World Scientific, River Edge, NJ, USA.

[35] Bourassa, A. E., C. A. McLinden, A. F. Bathgate, B. J. Elash, and D. A. Degenstein (2012a), Precision estimate for Odin-OSIRIS limb scatter retrievals, Journal of Geophysical Research: Atmospheres, 117, D04303, doi:10.1029/2011JD016976.